OPTICAL PROPERTIES FOR LUNG CANCER MARGIN DETECTION

TIME RESOLVED FLOURESCENCE AND DIFFUSE REFLECTANCE MEASUREMENTS FOR LUNG SQUAMOUS CARCINOMA TUMOR MARGINS

By SARAH COSTA, B.Sc.

A Thesis Submitted to the School of Graduate Studies in Partial Fulfillment of the Requirements for the Degree Master of Medical Physics

McMaster University © Copyright by Sarah Costa, June 2023

McMaster University MASTER OF SCIENCE (2023) Hamilton, Ontario (Medical Physics)

TITLE: Time Resolved Fluorescence and Diffuse Reflectance Measurements for Lung Squamous Carcinoma Tumor Margins

AUTHOR: Sarah Costa,
B.Sc. (McMaster University)

SUPERVISOR: Dr. Michael Farquharson

NUMBER OF PAGES: viii, 38

Lay Abstract

Lung cancer is the leading cause of death from cancer and is typically treated by surgically removing the tumor. To improve survival all cancer cells must be removed which can be challenging. This project uses light to extract properties that can differentiate cancerous and non-cancerous lung tissue. These differences could be used during surgery to ensure no cancer cells remain. The project tests this system on 36 tumor, 36 fibrotic and 9 normal lung tissue samples. Most parameters showed significant differences between tumor and other tissue types. Given that often times the surgical boundaries are between tumor and fibrotic tissue the results demonstrate promise in implementing this system. Future work using fresh samples would develop the system further and bring it one step closer to being used during surgery.

Abstract

Lung cancer is the leading cause of death from cancer in Canada and is typically treated with surgical resection of the tumor. To ensure good prognosis and limit metastases no cancer cells can be left behind during resection. This project uses time-resolved fluorescence and diffuse reflectance to differentiate cancerous and non-cancerous lung tissue. These differences could be used during surgical resection of tumor to ensure no positive margins are present. Using a bi-modal spectroscopy device, BEAR, optical properties were determined for 36 tumor, 36 fibrotic and 9 normal lung tissue samples. Most optical parameters showed statistically significant differences between tumor and other tissue types. Metabolic based optical parameters showed statistically significant differences between fibrotic and normal tissue while non-metabolic based parameters showed no difference. As surgical margins are likely to be between tumor and fibrotic tissue the results demonstrate success and promise for implementing this system. Future work using fresh samples would develop the system further and would be a step closer to *in vivo* use during surgery.

Acknowledgements

I would like to start off by thanking Dr. Mic Farquharson. It has been a pleasure working with you throughout my master's research. You have given me the space to work independently and on my own timeline which I will forever be grateful for. When I was stuck or needed some guidance you were quick to respond to my emails and set up meetings to discuss whatever was on my mind. I truly believe this experience would not have been as enjoyable if I had had a different supervisor. I wish you all the best on future work and look forward to hearing about the other successes in the lab.

Thank you Dr. Tom Farrell and Dr. Qiyin Fang for being part of my supervisory committee. I appreciate your guidance during our meetings and for accommodating my early defense date.

Thank you to Erica Dao! Without you I don't think I would have made it through this thesis. You have received the most emails with questions and concerns throughout my entire masters and have guided me every step of the way. Whenever I had a problem, you were quick to help me come up with solutions. I appreciate all the time you took teaching me how to use the BEAR system and prepping samples. I have learned so much from you over the past couple years and can't wait to hear about all your successes during your career.

Finally thank you to my support group at home including my closest friends, my parents, my brother, and my fiancé. You have all shaped me into the person I am today. Thank you for your guidance and for helping me through the up and downs of this master's degree. Luke thank you for reminding me why I went into this research in the first place. Your love and support has helped me through these last few years, and I couldn't have done any of this if you were not by my side. Thank you to my mom and dad for supporting me both emotionally and financially throughout my university career. Without your support I would not have had the courage to continue in my schooling and complete a graduate degree. Without you both I would not be where I am today, and I am so very grateful for that.

Table of Contents

List of Figures and Tables

List of Acronyms and Symbols

TRF- Time resolved fluorescence
DR-diffuse reflectance
NSCLC - non-small cell lung cancer
BEAR-Biological emission and reflectance
ns – nanoseconds
nm – nanometers
μ_a – absorption coefficient
τ – fluorescence lifetime
μ_s – scattering coefficient
μ_s' - reduced scattering coefficient
g – anisotropy factor
CT – computed tomography
MRI – magnetic resonance imaging
PET – positron emission tomography
NIR – near infrared
NADH – reduced form of nicotinamide adenine dinucleotide
FAD – flavin adenine dinucleotide
OCT – Optical coherence tomography
I – intensity
I_o – maximum intensity
a.u. – arbitrary units
FWHM – full width half maximum
H&E – hematoxylin and eosin
FLIM – fluorescence lifetime imaging
BSA – Bovine Serum Albumin

Declaration of Academic Achievement

I declare that this thesis was composed by myself and that the work is my own except where explicitly stated in the text. I declare that the work has not been submitted for any other degree and does not involve plagiarism or academic dishonesty.

Chapter 1: Introduction

This study investigates how squamous carcinoma of the lungs has different optical properties than normal and fibrotic tissue. By using time resolved fluorescence (TRF) and diffuse reflectance (DR) the optical properties, fluorescence intensity, fluorescence lifetime, absorption and reduced scattering coefficients, can be determined.

1.1 Motivation

This project focuses on differentiating cancerous from noncancerous lung tissue using optical properties. Similar studies have been performed with the existing equipment to compare cancerous and noncancerous breast tissue. The aim of this study is to determine the feasibility of using the same equipment for different tissue types, in this case lung tissue. The results from the breast study show that the difference between tissues across all optical properties measured are statistically significant [1,2]. Another research group has combined TRF and DR into one probe to assist in biopsy extraction for lung cancer [3,4]. This method however has not been used for margin detection during surgery. By combining the two modalities, a more accurate picture of our samples can be established and would not increase the processing time significantly.

1.2 Lung Squamous Carcinoma

In Canada lung cancer is the most commonly diagnosed cancer and is the leading cause of death from cancer [5]. Lung cancer can be separated into two categories, small cell lung cancer and non-small cell lung cancer (NSCLC). Small cell is a systemic disease and therefore has no cure while NSCLC can be removed with surgery if detected early enough [6]. The type of surgery depends on tumor properties including size, location, and invasiveness [7]. Removing an entire lobe (lobectomy) is the most common surgery except in cases where patients have limited pulmonary function prior to surgery [6]. There is an inverse relationship between amount of normal lung tissue removed and functionality in tissue post-surgery [8].

Non-small cell lung cancer accounts for 85% of all lung cancers. NSCLC can be further divided into adenocarcinoma (50% of cases), squamous carcinoma (30% of cases), and other [9]. New treatments have been shown to greatly benefit those diagnosed with adenocarcinoma including some non-surgical options. However, the same cannot be said for squamous carcinoma[9]. Tumor microenvironments are made up of extracellular matrix proteins, tumor-associated cells, and vasculature [10]. Metastasis is a process where tumors begin local invasion

and migration followed by intravasation which allows the tumor cells to enter the blood stream and embed themselves in distant tissue [10]. The Warburg effect is a classic sign of cancer as it occurs when cells switch from oxidative phosphorylation to aerobic glycolysis despite oxygen being available [11]. Tumors have been found to change their metabolic pathway easily and use other nutrients apart from glucose as a fuel source [11].

1.3 Tumor Margins

When looking at surgical resection of tumors there are two terms to consider, surgical margins and tumor margins. The tumor margins are the regions where the tumor is touching non-cancerous tissue. Surgical margins are the regions where the surgeon actually cuts. A positive surgical margin is one in which there is still cancerous tissue, this can either be on the microscopic or macroscopic level. Negative surgical margins mean there is no cancerous tissue and therefore likely no cancer left behind. In an ideal world the tumor margins and surgical margins are the same. However, this is incredibly challenging as cancerous tissue looks similar to non-cancerous tissue to the naked eye. Because of this surgeons often choose to remove more tissue than is necessary, to ensure all the tumor is removed. Despite excess tissue being removed there often still is positive surgical margins in lung cancer surgery [12]. One way to combat this is to send samples of excised tissue to histology for analysis during surgery. Histological analysis during surgery would require patients to remain open on the table for long periods of time which has been linked to higher mortality rates [13]. This makes this option not feasible and therefore another modality is required.

Positive margins in NSCLC surgery occur in 5-15% of cases and have been shown to negatively impact patient outcome [14]. Positive margins may lead to both local and distant disease recurrence. Incomplete resection halves the 5-year survival rate and is more problematic for those in the early stages of this cancer [14]. Given that we are able to detect lung cancer earlier than previously through the use of low-dose CT screening [15] achieving negative margins is even more important. Eighty three percent of patients who had negative margins showed disease free survival at 5 years compared to 30.8% of patients who had positive margins [14].

While increased surgical margins has shown lower rates of relapse [14] leaving behind as much normal tissue as possible has shown better lung functionality [16]. The challenge is to decide if removing more tissue and potentially removing all tumor is better than leaving more normal tissue behind and improving functionality and presumably quality of life post-surgery. If a

system is developed that can inform surgeons that all the tumor has been excised and therefore no more cutting is required, this can allow for more informed decisions in such a debate. Segmentectomy which requires more thoughtful cutting has shown significant benefits over wedge resection [14] and lobectomy [16] further proving this point. This type of detection would be especially beneficial when looking at tumors situated along airways and major blood vessels as these structures need to be left behind. Additionally, for those with comorbidities leaving behind normal tissue would allow for better functionality post-surgery. Finally, if an entire lobe is removed this type of device could be used to confirm that the remaining lobes are cancer free.

1.4 BEAR system

Other research group members use diffuse reflection (DR) and time-resolved fluorescence (TRF) to determine cancerous and non-cancerous optical properties. This bi-modal system is called the biological emission and reflectance (BEAR) system. By comparing these results one can differentiate cancerous and non-cancerous tissues in real time. These optical properties can determine tissues' structural and biochemical information. When light hits a surface and reflects at various angles it is undergoing DR. This reflectance can then be measured and analyzed in a MATLAB code to find structural abnormalities. When molecules are excited by incoming light and then return to their ground state fluorescence occurs. TRF determines the fluorescence intensity and lifetime in endogenous fluorophores. Fluorescence lifetime is the time it takes for a population of excited fluorophores to return to their ground state. This is an intrinsic property and follows an exponential decay curve. The fluorescence intensity is how much light the population is emitting. Tumors differ in their function, structure, and biochemical properties from their normal counterparts [17]. Both DR and TRF can independently differentiate the normal and tumor tissue [3,4,18,19,20] however combining the two optical systems can result in more accurate categorization. Additionally using both modalities allow for using data from one modality to correct the other modality. For example, DR is used to determine absorption and reduced scattering coefficients of a tissue while TRF can determine the fluorescence of the same tissue. By knowing the absorption properties, the intrinsic fluorescence of the tissue can be determined thus making it easy to compare regardless of where the system is set up [21].

1.5 Challenges

As with any study there are some challenges when conducting this research. In this study there was limited access to true normal samples. Given that all of our patients were smokers much of

their lungs showed fibrosis, a common comorbidity for lung cancer[22,23]. This meant getting more samples from the tumor bank to find true normal samples to compare. These normal samples did not come from the same patients and therefore matched pair testing could not be used. The probe was not set to the same distance from the sample each time and to limit the variability the probe was positioned as close to the sample as possible without touching the sample. Additionally, the intensity values were normalized to the mean NADH (460nm) intensity to account for any errors that may be associated with this difference. In order to compare tissue types 100% tissue composition is required whether looking at tumor or noncancerous tissue. To do this, histology was performed and overlayed with the scan to ensure the point of interest matched the tissue type of choice. This can lead to some slight variation in the histology versus what was measured as the sample's size and orientation changes slightly during processing and the overlay is using the operators best match. This error was reduced however as most of the tissue was uniform and by only using points of interest that were surrounded by the same tissue type.

1.6 Overview

Chapter 2 provides background on the main topics for this project. The chapter starts by giving an overview of cancer biology including characteristic traits. It goes through the normal lung anatomy before discussing lung cancer specifically. The chapter briefly mentions the various lung cancer types and some key components of each type. How light interacts with tissue is discussed and the chapter goes more in depth on the interactions being manipulated in this project. The chapter concludes with discussions on tissue analysis techniques and different optical spectroscopy techniques.

Chapter 3 explains the methodology used in this project and gives a breakdown of the samples used. The sample preparation required for the use of the optical system is explained as is the use of the raster scanning method for data collection. The list of optical measurements extracted is stated as well as an explanation for how the system extracts the properties.

Chapter 4 includes the results of the experiment as well as the discussion. This chapter has various tables that show the values for fluorescence intensity, fluorescence lifetime, absorption coefficient and reduced scattering coefficient for all three tissue types. This chapter also shows the results of the Wilcoxon ranked sum test for each of these properties when comparing the tissue types. The fluorescence intensity and fluorescence lifetime data can be easily visualized

with the box plots in this section. The absorption and reduced scattering coefficient results are shown in graphs with respect to wavelength. Additionally, the values for the wavelengths of interest (540nm and 576nm) can be visualized through histograms in this chapter.

Chapter 5 gives a summary of the major findings of the project. The limitations and future steps are also discussed in this chapter. The chapter ends with concluding remarks.

References

[1] E. Dao, "X-ray and Optical Techniques for Classification & Characterization of Tissue for Applications in Cancer," McMaster University, Hamilton ON. 2022.

[2] N. Shalaby, A. Al-Ebraheem, V. N. D. Le, S Cornacchi, Q Fang, T Farrell, P. Lovrics, G. Gohla, S. Reid, N. Hodgson, and M. Farquharson, "Time-resolved fluorescence (TRF) and diffuse reflectance spectroscopy (DRS) for margin analysis in breast cancer," Lasers in Surgery and Medicine, vol. 50, pp. 236-245. 2018.

[3] J. W. Spliethoff, D. J. Evers, H. M. Klomp, J. W. van Sandick, M. W. Wouters, R. Nachabe, G. W. Lucassen, B. H. W. Hendriks, J. Wesseling, and T. J. M. Ruers, "Improved identification of peripheral lung tumors by using diffuse reflectance and fluorescence spectroscopy," Lung cancer, vol. 80, pp. 165-171. 2013.

[4] D. J. Evers, R. Nachabe, H. M. Klomp, J. W. van Sandick, M. W. Wouters, G. W. Lucassen, B. H. W. Hendriks, J. Wesseling, and T. J. M. Ruers, "Diffuse reflectance spectroscopy: a new guidance tool for improvement of biopsy procedures in lung malignancies," Clinical Lung Cancer, vol. 13, pp. 424-431. 2012.

[5] C. C. S. A. Committee, "Lung Cancer Statistics," Canadian Cancer Society, 2020.

[6] J. Handy, J. Asaph, L. Skokan, C. Reed, S. Koh, G. Brooks, C. Douville, A. Tsen, G. Ott, and G. Silvestri, "What happens to patients undergoing lung cancer surgery?: Outcomes and quality of life before and after surgery," Chest, Vol. 122, pp. 21-30, 2002.

[7] C. C. S. A. Committee, "Surgery for Non-Small Cell Lung Cancer," Canadian Cancer Society, 2020.

[8] H. Harada, M. Okada, T. Sakamoto, H. Matsuoka, and N. Tsubota, "Functional Advantage After Radical Segmentectomy Versus Lobectomy for Lung Cancer," The Annals of Thoracic Surgery, Vol. 80, pp. 2041-2045, 2005.

[9] P. Perez-Moreno, E. Brambilla, R. Thomas, and J. Soria, "Squamous Cell Carcinoma of the Lung: Molecular Subtypes and Therapeutic Opportunities Lung SCC: Molecular Subtypes and Therapeutic Opportunities," Clinical Cancer Research, Vol. 18, pp. 2443-2451, 2012.

[10] P. P. Provenzano, K. W. Eliceiri, and P. J. Keely. "Multiphoton microscopy and fluorescence lifetime imaging microscopy (FLIM) to monitor metastasis and the tumor microenvironment," Clinical & Experimental Metastasis, Vol. 26, pp. 357-370. 2009.

[11] M.M. Lukina, L. E. Shimolina, N. M. Kiselev, V. E. Zagainov, D. V. Komarov, E. V. Zagaynova, and M. V. Shirmanova. "Interrogation of tumor metabolism in tissue samples ex vivo using fluorescence lifetime imaging of NAD (P) H," Methods and Applications in Fluorescence, vol. 8, pp. 014002. 2019.

[12] A.G. Little, V. W. Rusch, J. A. Bonner, L. E. Gaspar, M. R. Green, W. R. Webb, and A. K. Stewart, "Patterns of Surgical Care of Lung Cancer Patients," The Annals of Thoracic Surgery, Vol. 80, pp.2051-2056, 2005.
[13] E. Korol, K. Johnston, N. Waser, F. Sifakis, H. Jafri, M. Lo, and M. Kyaw, "A Systematic Review of Risk Factors Associated with Surgical Site Infections Among Surgical Patients," PloS one. Vol. 8, pp. e83743, 2013.
[14] J. Predina, J. Keating, N. Patel, S. Nims, and S. Singhal. "Clinical implications of positive margins following non-small cell lung cancer surgery," Journal of Surgical Oncology, Vol. 113, pp. 264-269. 2016.
[15] P. F. Pinsky, "Lung cancer screening with low-dose CT: a world-wide view," Translational Lung Cancer Research, Vol. 7, pp. 234-242. 2018.
[16] H. Harada, M. Okada, T. Sakamoto, H. Matsuoka, and N. Tsubota, "Functional Advantage After Radical Segmentectomy Versus Lobectomy for Lung Cancer," The Annals of Thoracic Surgery, Vol. 80, pp.2041-2045, 2005.
[17] L. Lansdowne, "Cancer Cells vs Normal Cells," Technology Networks Cancer Research, 2020.
[18] M. Wang, F. Tang, X. Pan, L. Yao, X. Wang, Y. Jing, J. Ma, G. Wang, L. Mi, "Rapid diagnosis and intraoperative margin assessment of human lung cancer with fluorescence lifetime imaging microscopy," BBA Clinical, Vol. 8, pp. 7-13. 2017.
[19] K. Awasthi, F. Chang, P. Hsieh, H. Hsu, and N. Ohta, "Characterization of endogenous fluorescence in nonsmall lung cancerous cells: A comparison with nonmalignant lung normal cells," Journal of Biophotonics, Vol. 13, pp. e201960210. 2020.
[20] M. Y. Berezin, and S. Achilefu. "Fluorescence lifetime measurements and biological imaging." Chemical Reviews Vol. 110, pp. 2641-2684. 2010.
[21] F. Badr, "Optical Biopsy Instrument Design and Parameter Extraction from Hyperspectral Time-Resolved Fluorescence Data," McMaster University, Hamilton ON, 2019.
[22] T. M. Alfaro, and C. R. Cordeiro, "Comorbidity in idiopathic pulmonary fibrosis-what can biomarkers tell us?" Therapeutic Advances in Respiratory Disease, Vol. 14, pp. 1753466620910092. 2020.
[23] B. Ballester, J. Milara, and J. Cortijo, "Idiopathic pulmonary fibrosis and lung cancer: mechanisms and molecular targets," International Journal of Molecular Sciences, Vol. 20, pp. 593. 2019.

Chapter 2: Background

2.1 Lung Anatomy and Cancer Biology

2.1.1 Cancer Biology

A review paper by Hanahan and Weinberg dictates that all types of cancer are defined by six common traits. The paper reduces cancer's complex nature to self-sufficient growth, resisting inhibitory growth signals, resisting programmed cell death, indefinite reproduction, angiogenesis, and tissue invasion [1]. These differences in mechanisms lead to physical and biochemical changes that could be used as markers for optical systems. Due to its ability to

grow without input from other cells, tumors show an increase in cell density compared with normal tissue. By resisting inhibitory growth signals cancer cells continue to divide even if there is not sufficient space in their surroundings. This could lead to irregular cell boundaries as they need to adjust their shape to fit. By resisting programmed cell death and dividing indefinitely cancer cells will continue to divide even if the DNA is damaged, unorganized or contains extra chromosomes. This leads to more cells with irregular DNA in the nucleus. In 2011 Hanahan and Weinberg added dysregulated metabolism, immune system avoidance, genome instability and inflammation to their list of cancer defining traits [2]. Changes in metabolism can be linked to changes in concentration and binding of biomolecules which can be detected with optical systems. Depending on the cancer type the way these common traits occur and interact changes. This means that while all cancers possess these characteristics, they are unique in their mechanism, timeline, and properties [2].

2.1.2 Lung Anatomy

The lungs are involved in oxygen exchange, where carbon dioxide leaves our bodies and oxygen enters the blood stream [4]. Humans have two lungs each separated by fissures into a series of lobes. The left lung has two lobes, the superior and inferior which is separated by the oblique fissure. The right lung has three lobes, the superior, middle, and inferior which are separated by the oblique and horizontal fissures. The lungs vary in their shape and size with the right lung being larger, shorter, wider, and heavier than the left lung. Additionally, the left lung contains the cardiac notch which allows the heart to fit in nicely. The right lung has vasculature grooves for the superior and inferior vena cava. The hilum of the lung is located in the middle between the lungs and acts as the root of the lung where structures enter and exit. The trachea connects the larynx to the bronchi which are the large airways of the lungs. As we get further into the lungs the airways continue to divide into smaller and smaller passages. The right bronchus splits into three secondary bronchi and the left bronchus splits into two secondary bronchi which divides again. The right lung has ten bronchopulmonary segments in total while the left has nine. As the divisions get smaller and smaller, they begin to be known as bronchioles which are the end of the conducting component of the air pathway. The terminal bronchioles become respiratory bronchioles which become alveolar ducts, sacs and then alveoli. The alveoli are the main respiratory component of the lungs, where gas exchange occurs. Pulmonary arteries carry poorly

oxygenated blood from the heart to the lungs then back to the heart to be sent to the rest of the body [4]. Figure 2.1[5] shows the lung anatomy including labels for the conducting component of the airways and a close up of the respiratory component.

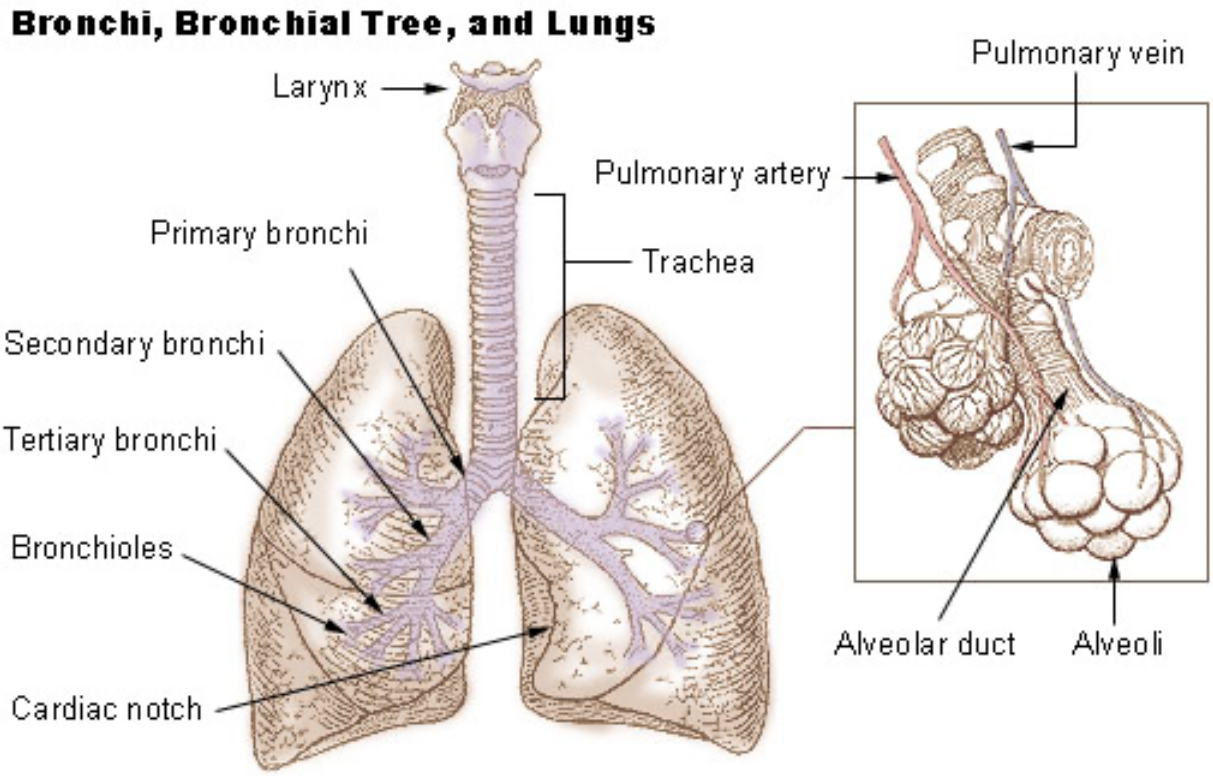

Figure 2.1: ***Anatomy of the human lung*** [5]

2.1.3 Lung Cancer

Lung cancer is the most commonly diagnosed cancer and has the highest mortality rate in Canada [3]. Lung cancer can be further subdivided into small cell lung cancer and non-small cell lung cancer (NSCLC). Additionally, NSCLC can be separated into squamous cell carcinoma, adenocarcinoma, and large cell carcinoma. Squamous cell carcinoma typically forms large tumors near the center of the lungs, close to the hilum while adenocarcinoma is typically found in the periphery. Large cell lung cancer is rare and shows no evidence of squamous differentiation, found in squamous carcinoma or glandular differentiation which is characteristic of adenocarcinoma [6]. Squamous differentiation includes intercellular bridges, keratinization, and keratin pearl formation [7]. Large cell lung cancer is usually found in the lung periphery and largely consists of necrotic tumor [7]. Small cell lung cancer is the most

aggressive type and leads to a significant number of metastasises [6]. It typically presents itself as a perihilar mass and is often found in a peribronchial location [7]. This project focuses on squamous cell carcinoma due to its prevalence and limited treatment plans associated with this cancer type.

As normal cells become cancerous there are some histological changes that appear in the tissue. Figure 2.2 shows the progression from normal lung tissue to squamous cell carcinoma. The first image shows normal bronchial epithelium. The cells are ciliated columnar cells, and each cell is connected to the basement membrane. This type of epithelium must be converted into squamous epithelium for cancer to occur, a process called metaplasia. Metaplasia occurs when epithelium is irritated, in the case of lung cancer often due to smoking. From there the squamous epithelium creates a basal layer that has been keratinized. Keratinization prevents water from entering the body from the outside or leaving from the inside. This is not present in normal lung tissue as there is no squamous epithelium. Squamous carcinoma can spread toward the bronchi entering and blocking the airway. It can invade along the bronchi towards the mediastinum or from the bronchi downward towards the bottom of the lungs. This final type of invasion typically leads to necrosis and hemorrhaging. As mentioned earlier squamous epithelium has two main histological characteristics, intercellular bridges which look like staples between cells and keratin pearl formation which is the most reliable feature but is not always present.

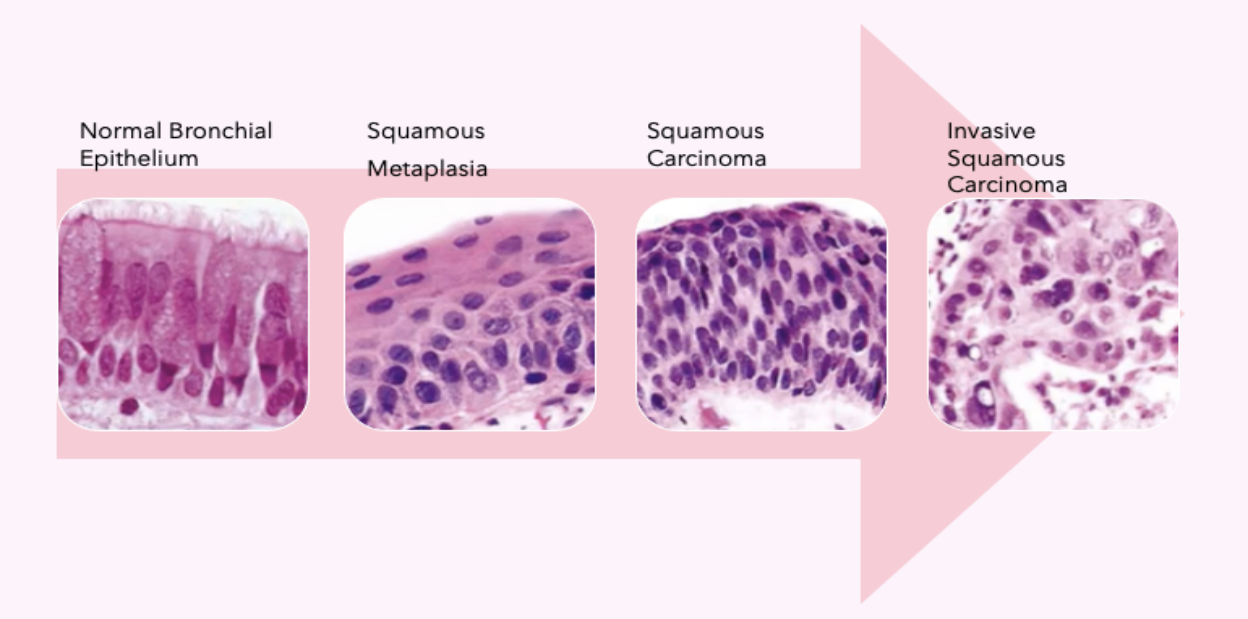

*Figure 2.2**: Squamous cell carcinoma lung cancer progression*** [8]

2.2 Light Interaction with Tissue

When a photon interacts with tissue it can undergo various mechanisms including transmission, reflection, scattering and absorption. Transmission is where the photons pass through the tissue. Scattering is a form of transmission where the photons pass through the tissue but not in the same direction as it was originally going. The amount of scattering that occurs depends on the properties of the incident light as well as the properties of the tissue. Reflection occurs when the photons pass through the tissue and escape the tissue in the opposite direction as the incident light path. If the observer was looking in the same direction as the direction of incident light, they would see the reflected light coming towards them back out of the tissue. Absorption occurs when the incident light does not continue through the tissue, nor does it come back to the observer. The light seems to have disappeared but has actually been turned into another form of energy.

When a photon interacts with various molecules within the tissue the photon can excite an electron from the ground state. An excited electron will either convert this energy into heat energy or by emitting a photon itself. The amount of absorption that occurs depends on the properties of the tissue and can be described by the absorption coefficient (μ_a). The absorption coefficient is the probability of absorption per unit path length and typically has a unit of cm^{-1}. There are two types of processes that can be occur as the excited electron returns to the ground state, phosphorescence, and fluorescence.

Phosphorescence typically takes longer to occur than fluorescence. Phosphorescence occurs when the excited electron undergoes intersystem crossing which causes it to change its spin state. This change in spin needs to be reversed before it can return to the ground state. Because of this transition there is a time delay which allows phosphorescence to occur even after the excitation light is no longer present. In contrast to phosphorescence, fluorescence occurs when the excited electron does not need to change its spin state to return to the ground state.

A simple Jablonski diagram is shown in figure 2.3. This diagram shows some of the transitions that can occur during absorption. Each transition occurs at different time scales with absorption/excitation being the fastest, femtosecond time scale, and phosphorescence being the slowest, microsecond or longer time scale. The time it takes for this excited electron to return to the ground state is the fluorescence or phosphorescence lifetime (τ).

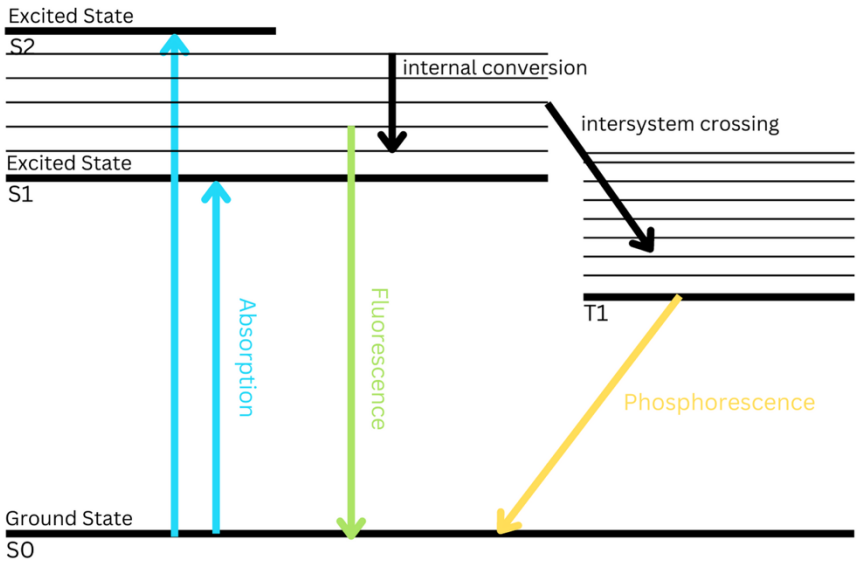

Figure 2.3: ***A simple Jablonski diagram showing electron transitions.***

Fluorescence occurs when an excited molecule, a fluorophore, returns to its ground state [9]. Autofluorescence is a fluorescence that occurs when the fluorophores of interest are naturally present in the biological tissue and therefore do not need to be added [10]. Changes in tissue microstructure as well as the concentration and distribution of endogenous fluorophores can influence the autofluorescence taking place. The changes can take place when a tissue transitions from normal to pathogenic. Autofluorescence emission can also be altered by metabolic, morphological and concentration changes. Additionally, the source parameters, geometry, and detection technique, can also influence autofluorescence [10]. Each fluorophore has its maximum excitation at a specific wavelength and emission at another wavelength. The emission wavelengths are always longer than the absorption ones due to there being an energy loss in the process [9]. This phenomenon is known as Stokes shift. There are some potential errors in fluorescence measurements including self-absorption, photobleaching, spectral shift due to temperature and pH [10]. Keeping excitation intensity low can minimize photobleaching [10]. Fluorescence lifetime is an intrinsic property and is independent of the fluorophores concentration but does depend on the microenvironment [9,11,12]. Each fluorophore varies in its spectral characteristics making them identifiable from one another [9]. Using a time-resolved fluorescence decay pattern one can easily separate fluorophores as the

lifetime can help differentiate them when the spectra overlap. The endogenous fluorophores that are easiest to determine are NADH, flavins, collagen and elastin, tryptophan and tyrosine, porphyrin, lipofuscins and melanin [9].

There are two types of reflection that can occur when incident light interacts with material, diffuse and specular. Specular reflection occurs when the material the incident light interacts with is smooth. In this case the reflection occurs at the same angle as the incident light comes in. Given that tissue is not a smooth material specular reflection is not the main type of reflection, instead more diffuse reflection occurs. In diffuse reflection the incident light and the light reflected can occur at various angles. As the light is able to penetrate the tissue diffuse reflection can occur either at the surface or within the tissue. The angle that the reflected light comes at follows the same principle as specular reflection. However, since the light is interacting with surfaces that are rough the incident angle is constantly changing. Figure 2.4 shows the difference between specular and diffuse reflection (on the surface and within the tissue).

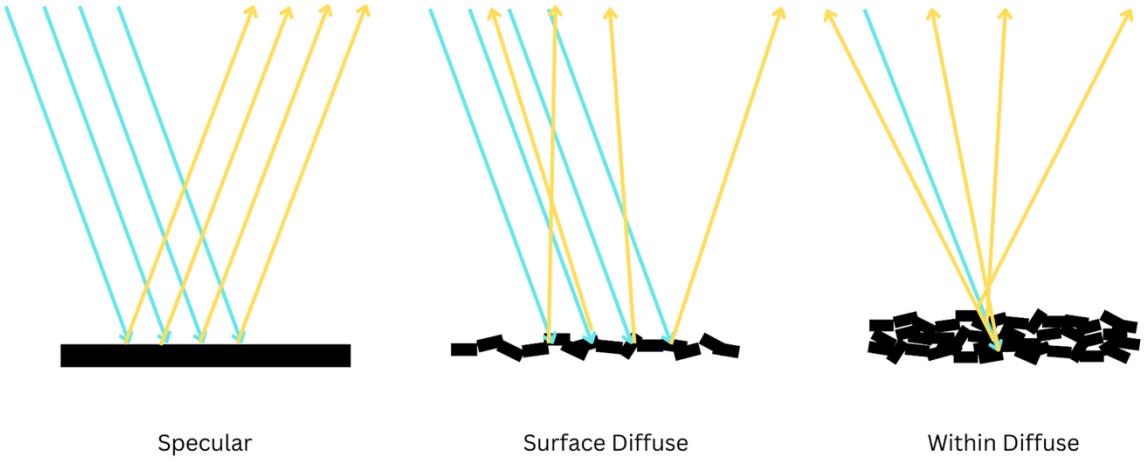

Figure 2.4: ***Specular and diffuse reflectance example.*** *Note: there is no change in wavelength of incident versus reflected light, colour change is just to differentiate the 2 (blue is incident light and yellow is reflected light).*

There are two types of scattering, elastic, and inelastic scattering. Elastic scattering occurs when there is no change in incident light wavelength and inelastic occurs with a change in incident photon wavelength. Scattering depends on the interactions between the incident light and the scatterer. Scattering may also occur more than once in tissue as there are multiple scatterers present.

During elastic scattering the incident light causes the scatterer to oscillate at the frequency of the incident light, this oscillation in and of itself causes the scatterer to emit a photon at its oscillating frequency. Because the scatterer is oscillating at the same frequency as that of the incident light it emits a new photon in any direction with the same wavelength. Elastic scattering can be further broken down into Rayleigh and Mie scattering. Rayleigh scattering occurs when the scatterers are smaller than the wavelength of the incident light. Mie scattering occurs when the scatterer is a homogenous sphere.

Inelastic scattering involves an energy change and can be broken down into Brillouin, Raman, inelastic x-ray scattering and Compton scattering. Brillouin, inelastic x-ray scattering, and Compton scattering are not relevant to this project. Raman scattering leads to a change in incident light direction as well as a wavelength change depending on the incident lights interaction with the scatterer. The wavelength change can either be due to a decrease in photon energy known as a stokes shift or the opposite can occur which is known as an anti-Stokes shift.

The probability of scattering per unit path length is the scattering coefficient (μ_s) and typically has a unit of cm^{-1}. Often times the reduced scattering coefficient (μ_s') which considers scattering angle is used instead. To account for the direction of scattering an anisotropy factor (g) is introduced where $g =< cos\theta >$, the average cosine of the scattering angle. If the photon scattering is not isotropic the reduced scattering coefficient will take this into account, such that $\mu_s' = \mu_s(1 - g)$.

2.3 Tissue Analysis Techniques

There are various cancer detection techniques used clinically or in research both at a macroscopic and microscopic level. Macroscopic techniques mostly include mechanisms used for diagnostic imaging including computed tomography (CT) scan, magnetic resonance imaging (MRI), and positron emission tomography (PET) scans.

2.3.1 Microscopic analysis techniques

On the microscopic level we can look at histological differences, differences in electrical properties or using molecular imaging to differentiate tumor from normal tissue. Histological differences between tumor and normal tissue include changes in cell shape and density, and irregularities in nuclei. This type of tissue analysis is the gold standard in cancer diagnosis. While histology is used to determine if surgical margins are clear of tumor cells it

is a time-consuming procedure and leaving a patient on the surgical table for longer increases risk of mortality [13].

Cancer cells and normal cells differ in their intra and extracellular pH, concentrations of calcium, potassium and sodium, transmembrane potential, and mitochondrial electrical properties. Tumor cells can survive in more acidic extracellular environments and have a more alkaline intracellular pH compared to normal cells. Proliferation, migration, and invasion all increase when there are ionic changes. Cancer cells have more sodium and water entering the cell whereas normal cells have higher intracellular potassium concentrations. Additionally, cancer cells allow more calcium to enter the cell. When considering transmembrane potential cancer cells have been shown to have lower capacitance values and an increase in negatively charged molecules on its outer surface. Mitochondrial pH is higher in cancer cells compared to normal cells [14]. All of these electrical property differences have led to various cancer therapies that use these differences to their advantage. A review by Di Gregorio et al. gives a comprehensive overview of current electrical therapies for cancer treatment [14]. These treatments include electrochemotherapy, irreversible electroporation, gene electrotransfer, and calcium electroporation. Electrochemotherapy uses electric impulses to improve chemotherapy drug delivery. Irreversible electroporation also involves electric impulses however the cellular membrane is not able to reseal after these impulses and therefore the cell dies. Gene electrotransfer is similar to electrochemotherapy but delivers nucleic acids as a form of gene therapy instead of cytotoxic drugs. Finally, calcium electroporation delivers calcium ions to cells as an increase in intracellular calcium has been found to induce apoptosis [14].

Molecular imaging uses fluorescence to visualize tumor margins. There are three types of labels typically used for this technique including fluorescent proteins, bioluminescence, and fluorescent dyes [15]. Bioluminescence and fluorescent proteins are engineered from cell lines or transgenic animals to carry genes that target the tissue of interest. Fluorescent dyes are able to specifically or unspecifically target the tissue without this additional complex step. There are various near infrared (NIR) fluorescent dyes used in tissue imaging applications each with unique features. Fluorescent dyes can be combined with specific substrates to create a probe that targets the tumor specifically. These probes have different functions that allow it to target the tissue of interest. These probes can either accumulate in the sentinel

lymph nodes, visualize increased cell metabolism, become activated by tumor-associated proteases, bind to a specific molecular target linked to the tumor or be used for vascular mapping [15]. These methods have all shown success in tumor margin assistance in research.

2.3.2 Optical Spectroscopy Techniques

Optical spectroscopy techniques allow for non-invasive analysis of the structural and biochemical changes associated with cancer progression. These techniques include Raman spectroscopy, fluorescence spectroscopy, diffuse reflectance spectroscopy and optical coherence tomography.

Raman spectroscopy uses Raman scattering to determine vibrational modes of molecules. This information creates a unique pattern that can be used to characterize the sample [16]. Spontaneous Raman scattering is extremely weak which is a limitation of this technique [16]. It uses monochromatic light to excite a sample which creates molecular vibrations based on the chemical bonds in the sample. As this light interacts with a sample there may be some changes in the wavelength depending on the characteristics of the sample. The wavelength can increase or decrease. Another limitation of this technique is using specific wavelengths of incident light to ensure fluorescence in the sample does not occur. Huang et al. uses NIR Raman spectroscopy to characterize bronchial tissue for lung cancer diagnosis [17]. The results of the study showed significant differences between normal and cancerous tissue. The cancerous tissue had a higher percentage signal for nucleic acids, tryptophan, and phenylalanine. Normal tissue had a higher percentage signal for phospholipids, proline, and valine [17]. McGregor et al. used Raman spectra for detecting malignant lung lesions with a sensitivity of 90% and specificity of 65% [16].

Fluorescence spectroscopy uses a laser light to excite fluorescent molecules, fluorophores, in a tissue that then emit photons at specific wavelengths. The system collects the emitted light and determines the fluorescence lifetime and intensity for each wavelength. This has been found to be useful in differentiating cancerous from non-cancerous tissue as these properties vary based on the tissue type. Currently clinical use of fluorescence bronchoscopy is common for lung cancer diagnosis [18]. Time resolved fluorescence (TRF) spectroscopy can either be in the frequency domain which records the phase and amplitude with respect to frequency of the light source or in the time domain which records intensity with respect to time. The frequency domain delivers the data in a shorter time period however the time

domain gives more accurate data [9]. In this project the time domain is used for the TRF data as the collection time is already short enough for our application and more accurate data would be helpful. Fluorophore concentration and location can give insight into cell and tissue function and alterations in function [12]. Fluorescence lifetime imaging can differentiate exogenous and endogenous fluorophores allowing us to determine metabolic states and discover potential optical biomarkers [11]. Using endogenous fluorophores allows researchers to observe changes in tissue structure without adding markers that may influence normal functioning [9]. The reduced form of nicotinamide adenine dinucleotide (NADH) and flavin adenine dinucleotide (FAD) are endogenous fluorophores that allow researchers to recognize highly active cells and increased metabolic activity which can be used to determine cancer or other pathogenic conditions [9,11]. Previous research has shown that the redox ratio (NADH/FAD ratio) varies in cancerous versus noncancerous cells both in lung tissue [19] and other organs [9]. The redox ratio is altered in transformed cells and therefore may indicate cancer invasiveness. Tumor cells are found to undergo enhanced glycolysis which is why the NADH, and FAD redox ratios are important to differentiate pathology [11]. Increased glycolysis can increase lactic acid levels causing a decrease in pH [11], which can change lifetimes. NADH is fluorescent in its reduced form but does not fluoresce when oxidized[9,20,21]. FAD is fluorescent only in its oxidized [9, 20] and free form [12, 21]. High FAD fluorescence intensity and longer lifetimes have been linked to invading metastatic cells [9,11]. Collagens and elastin are found in the extracellular matrix and are attenuated in tumors [9]. In some cases, increased stromal collagen has been linked to tumor formation and more invasive phenotype likely stemming from the fact that higher collagen density is related to tumorigenesis, local invasion, and metastasis [9]. Collagen has a broad emission spectrum up to 500nm and is dependent on the excitation wavelength [21]. There are other endogenous fluorophores that have been used in cancer margin detection but will not be used in this project. Tryptophan and tyrosine were linked to differences in excitation spectra at 340nm emission for malignant and normal cells [22]. There was an elevation of tryptophan in cancer cells likely due to upregulation of its transporter [22]. Tumor-localizing porphyrins can also be identified by their fluorescence lifetimes [9]. There are higher concentrations of protoporphyrin IX in cancer [9]. Fluorescence lifetime is lower for porphyrins *in vivo* compared to free in solution and the efficiency of emission depends on light conditions [21]. In

cancer cells there is an increased concentration of porphyrins and therefore enhanced autofluorescence around 630nm [21]. Melanin fluorescence lifetime is typically around 8ns and there is a difference in fluorescence lifetime in healthy skin and cancerous skin [12]. Fluorescence lifetime can differentiate healthy, basal cell carcinoma and melanoma in ex vivo samples. This is due to a difference in fluorescence lifetime of keratinocytes and melanocytes [12].

Diffuse reflectance (DR) spectroscopy uses a broad band light source on a sample and collects the diffuse reflectance off the sample at various collection distances. This diffuse reflectance can come from the rough surface of the sample or from within the sample as shown in section 2.2. In lung tissue this difference in reflectance between samples can show difference in the size, shape, and density of scatterers within the sample. These scatterers include whole cells, nuclei or organelles depending on the wavelength of incident light. The diffuse reflectance spectroscopy measurements can be used to generate the absorption and scattering coefficients of the sample. Various studies have found differences between tumor and normal lung tissue using DR spectroscopy [23,24,25]. Spliethoff et al. discriminated between lung parenchyma and tumor tissue with DR spectroscopy with a sensitivity of 98% and specificity of 86% [23]. Using ex vivo analysis with a DR spectroscopy system Evers et al. were able to differentiate tumor and normal lung tissue with 89% and 79% sensitivity and specificity respectively [24].

Optical coherence tomography (OCT) is used for imaging internal microstructures in tissue. It uses the echo time delay and backscattering of light to define structures. This process utilizes light interference to determine differences between reference reflected light and light reflected by the sample. A review paper by Van Manen et al. found OCT to be useful in diagnosis and intraoperative detection for malignancies in various cancers including lung cancer [26]. Hariri et al. used OCT to diagnose lung carcinomas and found the specificity and sensitivity to vary depending on the lung cancer type [27]. The sensitivity and specificity were 80.3% and 88.6% for adenocarcinoma, 83.3% and 87.0% for squamous cell carcinoma, and 85.7% and 97.6% for poorly differentiated carcinoma respectively [27].

References

[1] R. A. Weinberg, and D. Hanahan, "The Hallmarks of Cancer," Cell, Vol. 100, pp. 57-70. 2000.

[2] D. Hanahan, and R. A. Weinberg, "Hallmarks of Cancer: The Next Generation," Cell, Vol. 144, pp. 646-674. 2011.
[3] C. C. S. A. Committee, "Lung Cancer Statistics," Canadian Cancer Society, 2020.
[4] K. Katrivesis, J. Elia, B. Etiz, K. Cooley-Rieders, S. Hosseinian, and S. Melucci, "An Overview of Lung Anatomy and Physiology," Mechanical Ventilation Amid the COVID-19 Pandemic, pp. 5–24. 2022.
[5] "Lung Anatomy," 2022. Physiopedia, URL: https://www.physio-pedia.com/index.php?title=Lung_Anatomy&oldid=298340.
[6] V. Ambrosini, S. Nicolini, P. Caroli, C. Nanni, A. Massaro, M. C. Marzola, D. Rubello, S. Fanti, "PET/CT Imaging in Different Types of Lung Cancer: An Overview," European Journal of Radiology, Vol. 81, pp. 988-1001. 2012.
[7] W. D. Travis, "Pathology of Lung Cancer," Clinics in Chest Medicine, Vol. 32, pp. 669-692. 2011.
[8] V. Kumar, A. K. Abbas, N. Fausto, J. C. Aster. "Robbins and Cotran Pathologic Basics of Disease 9th Edition," Elsevier Health Sciences. 2014.
[9] D. Chorvat, and A. Chorvatova. "Multi-wavelength fluorescence lifetime spectroscopy: a new approach to the study of endogenous fluorescence in living cells and tissues." Laser Physics Letters, Vol. 6, pp. 175-193. 2009.
[10] R. S. DaCosta, H. Andersson, and B. C. Wilson. "Molecular Fluorescence Excitation–Emission Matrices Relevant to Tissue Spectroscopy," Photochemistry and Photobiology, Vol. 78, pp. 384-392. 2003.
[11] P. P. Provenzano, K. W. Eliceiri, and P. J. Keely. "Multiphoton microscopy and fluorescence lifetime imaging microscopy (FLIM) to monitor metastasis and the tumor microenvironment." Clinical & Experimental Metastasis. Vol. 26, pp. 357-370. 2009.
[12] P. Sarder, D. Maji, and S. Achilefu, "Molecular probes for fluorescence lifetime imaging," Bioconjugate Chemistry, Vol. 26, pp. 963-974. 2015.
[13] E. Korol, K. Johnston, N. Waser, F. Sifakis, H. Jafri, M. Lo, and M. Kyaw, "A Systematic Review of Risk Factors Associated with Surgical Site Infections Among Surgical Patients." PloS one. Vol. 8, pp. e83743, 2013.
[14] E. Di Gregorio, S. Israel, M. Staelens, G. Tankel, K. Shankar, and J. A. Tuszyński, "The distinguishing electrical properties of cancer cells," Physics of Life Reviews, Vol. 43, pp. 139-188. 2022.
[15] E.A. te Velde, T. Veerman, V. Subramaniam, and T. Ruers, "The use of fluorescent dyes and probes in surgical oncology," European Journal of Surgical Oncology (EJSO), Vol. 36, pp. 6-15. 2010.
[16] H. C. McGregor, M. A. Short, A. McWilliams, T. Shaipanich, D. N. Ionescu, J. Zhao, W. Wang, G. Chen, S. Lam, and H. Zeng, "Real-time endoscopic Raman spectroscopy for in vivo early lung cancer detection," Journal of Biophotonics, Vol. 10, pp. 98-110. 2017.
[17] Z. Huang, A. McWilliams, H. Lui, D. I. McLean, S. Lam, and H. Zeng, "Near-infrared Raman spectroscopy for optical diagnosis of lung cancer," International Journal of Cancer, Vol. 107, pp. 1047-1052. 2003.
[18] H. Zeng, A. McWilliams, S. Lam, "Optical spectroscopy and imaging for early lung cancer detection: a review," Photodiagnosis and Photodynamic Therapy, Vol. 1, pp. 111-122. 2004.

[19] M. Wang, F. Long, F. Tang, Y. Jing, X. Wang, L. Yao, J. Ma, Y. Fei, L. Chen, G. Wang, and L. Mi, "Autofluorescence Imaging and Spectroscopy of Human Lung Cancer'" Applied Sciences. Vol. 7, pp. 32. 2017.
[20] R. Penjweini, B. Roarke, G. Alspaugh, A. Gevorgyan, A. Andreoni, A. Pasut, D. L. Sackett, and J. R. Knutson. "Single cell-based fluorescence lifetime imaging of intracellular oxygenation and metabolism." Redox biology, Vol. 34, pp. 101549. 2020.
[21] M. Y. Berezin, and S. Achilefu. "Fluorescence lifetime measurements and biological imaging." Chemical reviews, Vol. 110, pp. 2641-2684. 2010.
[22] M. Atif, M. S. AlSalhi, A. A. AlObiadi, and A. S. Aldwayyan. "Fluorescence spectra of cultured normal and malignant lung cells." Laser Physics. Vol. 22, pp. 1353-1357. 2012.
[23] J. W. Spliethoff, D. J. Evers, H. M. Klomp, J. W. van Sandick, M. W. Wouters, R. Nachabe, G. W. Lucassen, B. H. W. Hendriks, J. Wesseling, and T. J. M. Ruers, "Improved identification of peripheral lung tumors by using diffuse reflectance and fluorescence spectroscopy," Lung Cancer, Vol. 80, pp. 165-171. 2013.
[24] D. J. Evers, R. Nachabe, H. M. Klomp, J. W. van Sandick, M. W. Wouters, G. W. Lucassen, B. H. W. Hendriks, J. Wesseling, and T. J. M. Ruers, "Diffuse reflectance spectroscopy: a new guidance tool for improvement of biopsy procedures in lung malignancies," Clinical Lung Cancer, vol. 13, pp. 424-431. 2012.
[25] S. Akter, M. G. Hossain, I. Nishidate, H. Hazama, and K. Awazu, "Medical applications of reflectance spectroscopy in the diffusive and sub-diffusive regimes," Journal of Near Infrared Spectroscopy, Vol. 26, pp. 337-350. 2018.
[26] L. van Manen, J. Dijkstra, C. Boccara, E Benoit, A. L. Vahrmeijer, M. J. Gora, and J. S. D. Mieog, "The clinical usefulness of optical coherence tomography during cancer interventions," Journal of Cancer Research and Clinical Oncology, Vol. 144, pp. 1967-1990. 2018.
[27] L. P. Hariri, M. Mino-Kenudson, M. Lanuti, A. J. Miller, E. J. Mark, and M. J. Suter, "Diagnosing lung carcinomas with optical coherence tomography," Annals of the American Thoracic Society, Vol. 12, pp. 193-201. 2015.

Chapter 3: Methodology

3.1 Samples

3.1.1 Sample Information

The samples used throughout this experiment were obtained from the Ontario Tumor Bank. There were 3 sample types used during the experiment: tumor, fibrotic, and normal lung tissue. The tumor and fibrotic tissue samples were extracted from patients who were diagnosed with squamous cell carcinoma. These samples were matched pair however some samples were too large for the sample holder and were split into 2 samples. These patients all underwent surgery after the diagnosis of squamous cell carcinoma of the lungs but before undergoing any other cancer treatment, including radiation. Patients were diagnosed with stage I or II squamous cell carcinoma and a metastatic stage of M0. The patients were ex-smokers between the ages of 60 and 90 with the median age being 72.5. There were complications in extracting true normal

lung tissue as upon histological examination the tumor adjacent normal was found to consist of fibrotic tissue. This was not surprising given that many patients diagnosed with lung cancer are comorbid with idiopathic fibrosis [1,2]. This means that the tumor boundaries during surgery are likely tumor and fibrotic tissue instead of tumor and normal. Although the clinical applications are still relevant, finding true normal samples could create a more in-depth database for the optical parameters. This meant obtaining new normal samples to compare optical properties. The new true normal samples were obtained from the same tumor bank however did not come from the same patients. The normal samples were chosen based on an archived histology slide database at the Ontario Tumor Bank. Histopathologists at the Ontario Tumor Bank confirmed that the samples were healthy normal lung tissue and sent digitized slides for approval before shipping the corresponding samples. This meant that only those that were 100% normal lung samples were accepted and a second histology after data collection was not necessary. In the end there were 36 tumor, 36 fibrotic (tumour adjacent normal) and 9 normal samples.

3.1.2 Fresh vs. Prefrozen

All of the samples used throughout the experiments were given to the lab from the Ontario Tumor Bank and arrived prefrozen as no fresh samples were available. While fresh samples would be ideal for this project given the clinical applications a study by Shalaby et al. showed that the optical properties were no different if the sample was fresh or prefrozen [3]. Shalaby et al. used 10 matched pair breast tissue samples and examined the samples under the optical system 30 minutes post-surgical extraction. The samples were then placed in a sub-zero refrigerator at -80 degrees Celsius for 4 to 6 weeks. At this point the samples were moved to room temperature and thawed within a few minutes without the need for additional heat. After running these defrosted samples through the optical system again Shalaby et al. found there to be no difference between the optical properties demonstrating this to be a reasonable procedure. As more freezing and defrost cycles occur some samples have demonstrated trouble holding their shape during sectioning which only affects the histology [4]. Because of these findings samples were limited to only 1 freeze thaw cycle however some samples underwent this cycle twice due to complications.

3.1.3 Optical system sample preparation

In order to collect optical data from the samples they are moved to a sample holder which is then placed in a sample mount just under the optical probe. Figure 3.1 shows the cross section of the probe. The sample holder is a 3D printed square with a 13mm diameter hole in the middle. The sample holders are made of white acrylonitrile butadiene styrene (ABS) and are 1mm thick. The thawed samples were sliced to fit within the sample holder volume and a thin ultralene film is used to cover both sides. This film does not affect the optical parameters but does allow the researcher to switch between samples without needing to clean the probe. This was done to streamline the data collection process. Once placed in the sample holder the samples were positioned in a 3D printed red polylactic acid (PLA) sample mount. The sample holders have a small hole at the top to ensure correct sample orientation each time. The small hole is used as a guide to determine where the probe should be located before the scanning process begins. Figure 3.2 shows each step in this process with figure 3.2 A-D pertaining to the steps prior to optical measurement.

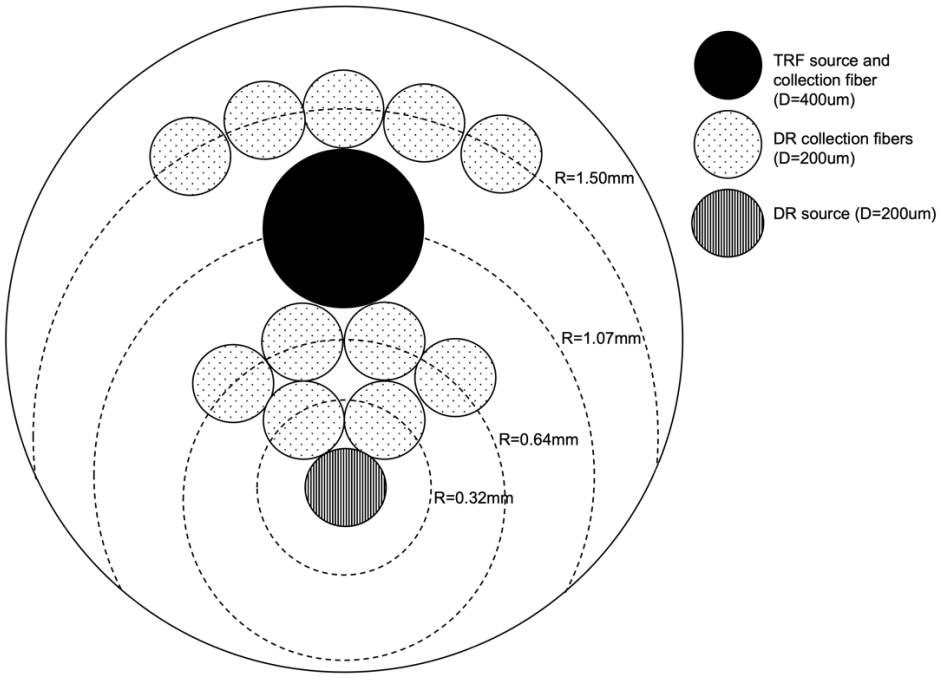

Figure 3.1 ***Cross-section of optical probe****. The entire probe is 3mm in diameter, The large black circle corresponds to the TRF source and collection fiber and is 400um in diameter. The bottom stripped circle corresponds to the DR source and is 200um in diameter. The remaining dotted circles correspond to the DR collection fibers located 0.32mm, 0.64mm, and 1.50mm away from the source.*

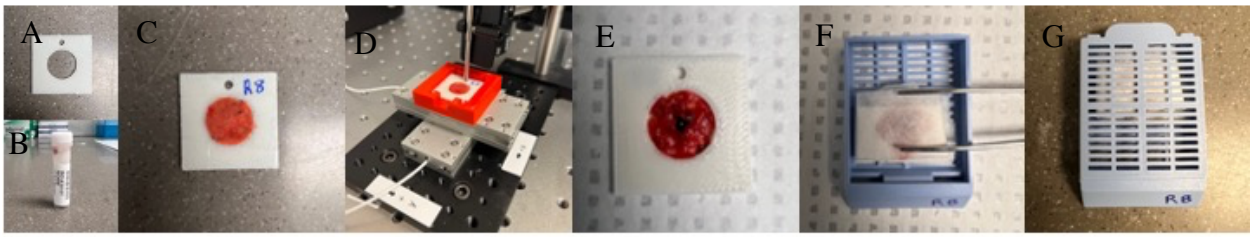

Figure 3.2 ***Methodology step breakdown. A.*** *sample holder,* ***B.*** *tube that contains the biological sample,* ***C.*** *sample holder with sample inside and ultralene film covering both sides,* ***D.*** *sample holder inside sample mount ready for optical system,* ***E.*** *sample flipped to reveal back with black ink dot,* ***F.*** *sample wrapped in lens paper,* ***G.*** *sample in histology cassette ready to be placed in formalin.*

Using a raster scanning method the data collection can occur at various points within the sample. The raster process starts in the top left corner of the sample and takes 12 1mm steps to the right at which point it takes 1 step down and then another 12 1mm steps to the left. This method ensures that no spot was measured more than once and allows an overlay of a grid which assists in sample histology matching. This ensures the optical spot measurements match with histological data.

While the intention is to use this grid method to match histology with the optical sample spot this grid is added visually when comparing images of the sample within the sample holder with the histology grid. This may have resulted in a slight difference in the orientation. However, the sample points that are classified as tumor, fibrotic or normal are typically surrounded by tissue of the same classification. This means that even if the grid is slightly shifted the overall classification would not have changed. The samples were overall homogenous and only samples of 100% composition were used when comparing parameters. Although each sample could have up to 169 sample points if the entire sample space was filled not all of them can be used.

After optical data collection, the samples undergo processing for histology. The front film is removed from the sample holder leaving the tissue sample exposed to the air. From there the sample holder is flipped into lens paper. This paper is used to ensure the tissue is oriented in the correct manner when placed in the tissue cassette. At this point the back film is removed and a small black ink dot is placed on the back of the sample. This told the people working in the histology lab which side is the back of the sample and ensures the histology slides come from the front as this is where the optical properties are extracted from. The sample is folded in the lens paper and placed in the tissue cassette so the sample is in the same orientation as when data collection took place. Figure 3.2 shows each step in this process with figure 3.2 E-G pertaining to the steps that occur after optical measurements. The samples are placed in 10% formalin for

24-48 hours and then transferred to 70% ethanol and transported to the histology lab. The samples undergo paraffin embedding and hematoxylin and eosin (H&E) staining. The sample slides are digitized to ease the tissue classification process.

3.2 Optical Measurements

3.2.1 TRF and DR components

The TRF component of the optical system uses a 355 nm, 300ps full width half maximum (FWHM) pulsed Nd:YAG laser. Using laser light allows for controlled excitation. The fact that the incident light is limited to our area of interest ensures that the remaining tissue is not excited which could lead to photobleaching. Photobleaching of the tissue would prevent extraction of the correct optical parameters. Additionally, the laser wavelength was chosen because of the types of fluorophores it excites in tissue. As discussed previously collagen, FAD and NADH fluorescence intensities and lifetimes have been shown to be different in diseased compared to normal tissue. By using this wavelength, all three fluorophores are excited simultaneously. This ensures all three can be used during classification without the need for additional excitation events.
The DR component uses a broadband xenon lamp. This allows for absorption and scattering for specific molecules and structures in the tissue sample. This wavelength range shows hemoglobin absorption as well as the nucleus and other extracellular matrix structures that cause scattering. A complication with using laser light on human tissue is that some lasers can cause tissue damage. This is true for lasers with high power and therefore the laser energy should be kept below 3uJ [4]. The laser used in this project is measured to be 2.6uJ which meets the power regulation.

3.2.2 Material information

In order for the system to work effectively it was ensured that the materials were contaminant free. This ensures low background noise which means the data collected was only from our sample and any differences between samples is attributed to the samples themselves. Additionally, the optical system including the collection fibers, sample holder, and sample mount must be made of non-fluorescing materials as this too would affect background noise. Samples are placed in an ABS white sample holder that had a hole all the way through. This sample holder was inexpensive but still sturdy enough to hold the sample and not break. As discussed earlier the sample was covered with ultralene film on both sides. This ensures that the holder does not contribute to background noise as it is not in the path of the beam behind the sample. The sample mount is made of red PLA and is within the beam path only after the beam goes

through the sample. This requires that the beam go through 1mm of tissue before interacting with the sample mount. This proves to not be an issue for the TRF component as the light cannot penetrate past the 1mm thick tissue however may have some effect on the DR component [4]. Given that the signal from the sample mount will have to travel back through the 1mm thick tissue the effect will be reduced even more which makes this signal negligible. If the area being measured did not have any sample present, then the light for both components would interact with the sample holder. However, given that these are not relevant to the data they are not useful and therefore the data points are omitted.

The optical system is set up in a room with ambient light sources. For these experiments all of the lights are turned off and the laptop brightness is reduced. This ensured all samples are measured using the same amount of light, almost zero. A sample was measured both with and without the lights and figures 3.3 and 3.4 show that both the TRF and DR component are not affected by ambient light, the differences are minimal. Once the system is moved to the surgical room the test should be performed again as the lights in there may be brighter and may require some accommodation.

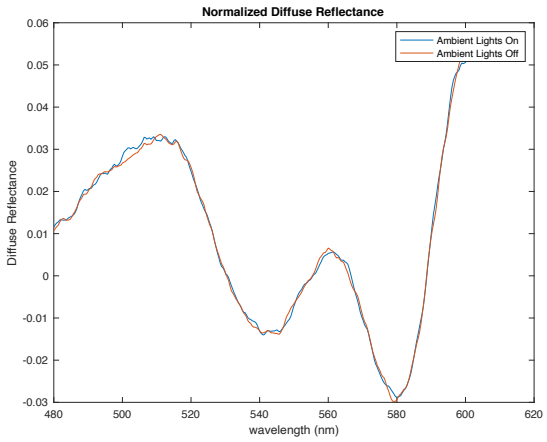

Figure 3.3 ***Normalized diffuse reflectance with and without ambient light***

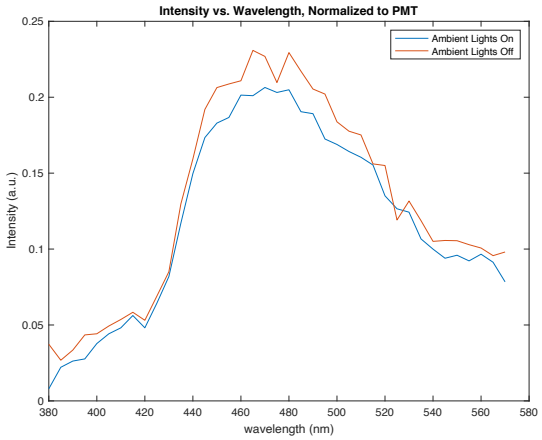

Figure 3.4 ***Intensity with respect to wavelength with and without ambient light***

3.3 Optical Parameter Extraction

This project uses custom MATLAB codes created by Erica Dao during her PhD to extract the parameters of interest [4].

3.3.1 Fluorescence intensity and lifetime

The TRF component of the optical system sends 11, 355nm laser pulses to the sample to excite the tissue. After each pulse the fluorescent light comes through the probe where it is processed further and enters a photomultiplier tube where the information gets digitized. The system saves the data as a .dat file which can be opened in MATLAB and processed further. The file consists of the signal intensity with respect to time for each wavelength and each pulse. Within the MATLAB code the bits are converted into mV. Each pulse is averaged and helps generate an average signal for each wavelength from 380-570nm in 5nm increments. Figure 3.5 shows the average signal for each wavelength on one graph and figure 3.6 shows the intensity for each wavelength. From there the decay portion of the average signal is extracted for the wavelengths of interest, 400, 460, and 515nm, and further processed. The data are fitted with an exponential curve and the intensity and lifetimes can be extracted from the decay curve coefficients. The intensity is found by taking the integral of this fitted function and the lifetimes are found by the exponential coefficient, τ, using equation 1.

[1] $$I = I_o e^{-t/\tau}$$

where I_o is the maximum intensity and τ is the fluorescence lifetime

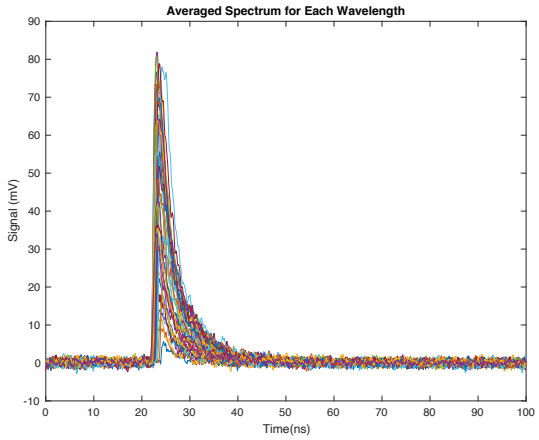

Figure 3.5 ***Average signal for each wavelength (380-570nm)***

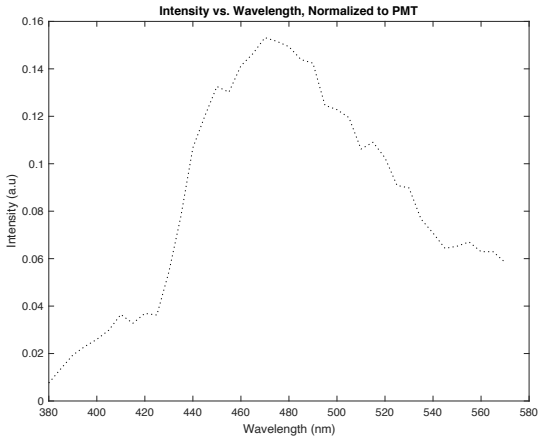

Figure 3.6 ***Intensity for each wavelength***

The fluorescence lifetimes and intensities are recorded for each wavelength of interest. The ability to extract these parameters from this simplified model has been debated however since the optical system results are being compared to itself for clinical application the true lifetimes and intensities are not necessary. All that is needed is to see the difference between diseased and normal for classification purposes. The fluorescence intensity is in arbitrary units (a.u.) and the intensity for FAD and collagen are normalized to NADH intensity. The FAD normalized to NADH intensity is also known as the redox ratio.

3.3.2 Diffuse Reflectance

For the DR component of the system a broadband light source shines on the sample and three sets of fibers collect the reflected light. These fibers are located at various distances from the light source. The data are saved in a .dat file with four columns, the first being the wavelengths measured and the last three being the intensity at each fiber distance for that wavelength.

Measurements were taken at 2nm increments from 480nm to 650nm. In order to calibrate the samples a 99% reflectance standard and a sample holder filled with deionized water are also recorded in the system. The water spectrum is used as a background check and is subtracted from each sample spectrum. Each sample spectrum was then normalized to the reflectance standard. There are various ways to extract absorption and reduced scattering coefficients, in this study indirect methods are used, specifically look up tables. Dao measured various phantoms in the optical system to generate a lookup table which is used for this project [4]. The phantoms were also put in a spectrophotometer to measure absorbance and by using Beer-Lambert law the absorption coefficient was determined. The lookup table creates a relationship between diffuse reflectance and the absorption and reduced scattering coefficients. This means that with each sample's given reflectance the MATLAB code that uses this lookup table can give the absorption and reduced scattering coefficients at each wavelength measured. The extracted coefficients are the total absorption coefficient and total reduced scattering coefficient. The absorption coefficient comes from the major absorbers in our sample, mainly hemoglobin and the reduced scattering coefficient comes from all the scatterers in the tissue, including whole cells and nuclei.

References

[1] B. Ballester, J. Milara, and J. Cortijo, "Idiopathic pulmonary fibrosis and lung cancer: mechanisms and molecular targets," International Journal of Molecular Sciences, Vol. 20, pp. 593. 2019.

[2] T. M. Alfaro, and C. R. Cordeiro, "Comorbidity in idiopathic pulmonary fibrosis-what can biomarkers tell us?" Therapeutic Advances in Respiratory Disease, Vol. 14, pp. 1753466620910092. 2020

[3] N. Shalaby, A. Al-Ebraheem, D. Le, S. Cornacchi, Q. Fang, T. Farrell, P. Lovrics, G. Gohla, S. Reid, N. Hodgson, and M. Farquharson, "Time-resolved fluorescence (trf) and diffuse reflectance spectroscopy (drs) for margin analysis in breast cancer," Lasers in Surgery and Medicine, vol. 50, pp. 236–245, 3 2018.

[4] E. Dao, "X-ray and Optical Techniques for Classification & Characterization of Tissue for Applications in Cancer," McMaster University, Hamilton ON. 2022.

Chapter 4: Results and Discussion

Given that next steps in this work would involve creating decision trees or other categorization models all results are recorded with standard deviation.

4.1 Fluorescence Lifetime

Table 4.1 shows the mean fluorescence lifetime and standard deviation for all three tissue types, normal, tumor and fibrotic for each wavelength of interest, 400nm, 460nm, and 515nm. Table 4.2 shows the Wilcoxon ranked sum test results comparing the tissue groups with each other. Figure 4.1 shows the box plots for each tissue type, normal, tumor, and fibrotic, for collagen, NADH and FAD mean fluorescence lifetime.

*Table 4.1**: Mean fluorescence lifetime (ns) and standard deviation for collagen, NADH and FAD for each tissue type***

	400nm (collagen)	460nm (NADH)	515nm (FAD)
Normal	3.06±0.6	3.39±0.4	3.57±0.4
Fibrotic	3.09±0.6	3.27±0.5	3.30±0.5
Tumor	2.89±0.6	2.89±0.5	2.92±0.5

*Table 4.2**: Wilcoxon ranked sum test results for mean fluorescence lifetime (ns) of collagen, NADH and FAD***

	400nm (collagen)	460nm (NADH)	515nm (FAD)
Normal vs. Fibrotic	0.9057	$P < 0.01$	$P < 0.01$
Fibrotic vs. Tumor	$P < 0.01$	$P < 0.01$	$P < 0.01$
Normal vs. Tumor	$P < 0.01$	$P < 0.01$	$P < 0.01$

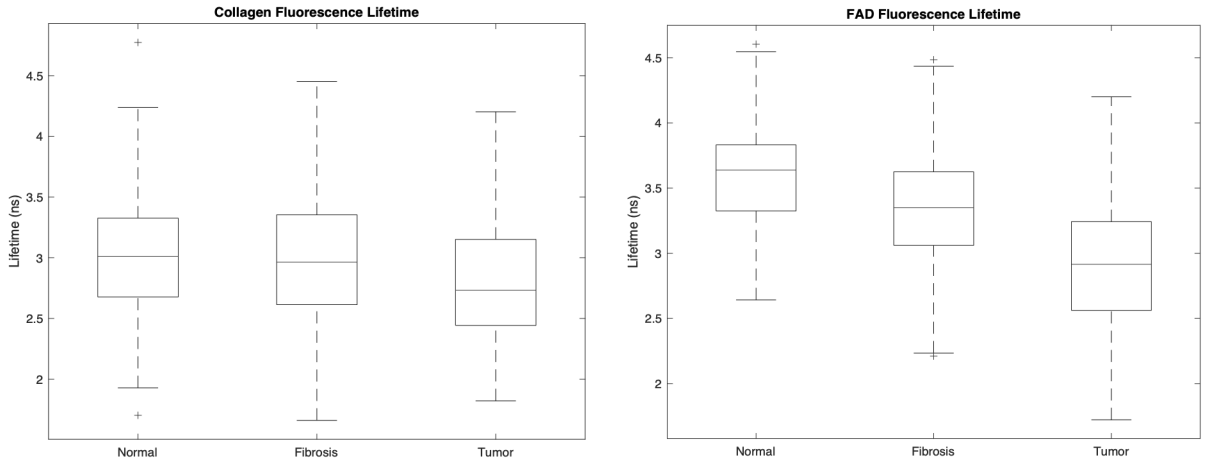

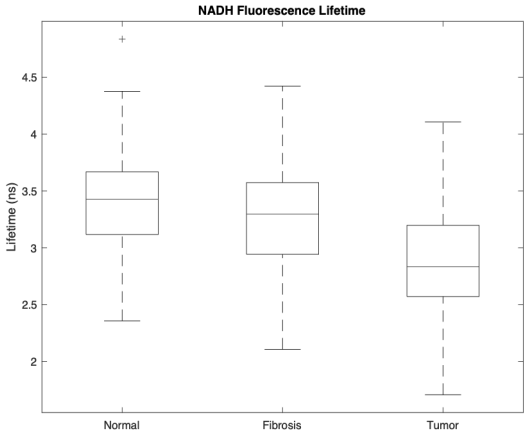

*Figure 4.1**: Box plots for fluorescence lifetime for collagen, NADH, and FAD for each tissue type.***

There are statistically significant differences in fluorescence lifetime for all three fluorophores when comparing tumor with the other tissue types. There are statistically significant differences in fluorescence lifetime for NADH and FAD when comparing fibrotic and normal lung tissue. There is no difference between collagen fluorescence lifetime when comparing fibrotic to normal tissue. The fluorescence lifetime decreased for tumor samples compared to normal and fibrotic tissue, which is consistent with previous literature [1,2,3]. NADH and FAD are used to determine changes in metabolism. These changes are likely due to the cells switching from oxidative phosphorylation to glycolysis in cancerous cells. It should be noted that current literature does not separate tumor adjacent normal into fibrotic and true normal. Therefore, there is no literature for fibrotic versus normal fluorescence lifetime. Collagen is related to tissue structure and organization. The structure and organization of tissue changes when the tissue undergoes tumor formation and collagen has been linked to tumorigenesis [4]. Based on this change in collagen it is expected that the tumor tissue shows statistically significant differences when compared with both fibrotic and normal lung tissue. Fibrosis is a result of lung scarring [5] that shows reduced tissue functionality. This means that there is likely a metabolic difference between fibrotic and normal lung tissue. This metabolic difference could be the reason we have statistically significant differences in NADH and FAD, metabolic coenzymes, lifetimes between the tissue types. The fact that fibrotic tissue lifetimes are shorter than normal lifetimes mean there is likely less oxidative phosphorylation occurring however the cells have not switched to anaerobic metabolism. When considering the fact that scar tissue does not grow or replicate this decrease in metabolism is expected [6]. Studies have reported longer collagen lifetimes with higher collagen

fibrils in diseased states [7]. In this case the collagen fluorescence lifetime is longer for fibrotic compared to normal tissue. This is expected as fibrosis is related to an increase in collagen presence in extra cellular matrix [8]. This difference however is not statistically significant. Depending on how far along the fibrosis is will determine how much additional collagen is deposited [8]. If the fibrosis is at its early stages, it may not have much more collagen than the normal samples which could be why the difference is not significant.

4.2 Fluorescence Intensity

Table 4.3 shows the mean fluorescence intensity for collagen and FAD normalized to NADH fluorescence intensity and standard deviation for all tissue types. Table 4.4 shows the Wilcoxon ranked sum test results for the normalized fluorescence intensity for comparing all groups to each other. Figure 4.2 shows the corresponding box plots for normalized fluorescence intensity of collagen and FAD.

*Table 4.3**: Mean normalized fluorescence intensity (a.u.) and standard deviation for collagen and FAD for each tissue type***

	Collagen/NADH	FAD/NADH
Normal	0.152±0.02	0.644±0.1
Fibrotic	0.158±0.03	0.680±0.1
Tumor	0.190±0.05	0.815±0.2

*Table 4.4**: Wilcoxon ranked sum test results for mean normalized fluorescence intensity (a.u.) for collagen and FAD***

	Collagen/NADH	FAD/NADH
Normal vs. Fibrotic	0.10	$P < 0.01$
Fibrotic vs. Tumor	$P < 0.01$	$P < 0.01$
Normal vs. Tumor	$P < 0.01$	$P < 0.01$

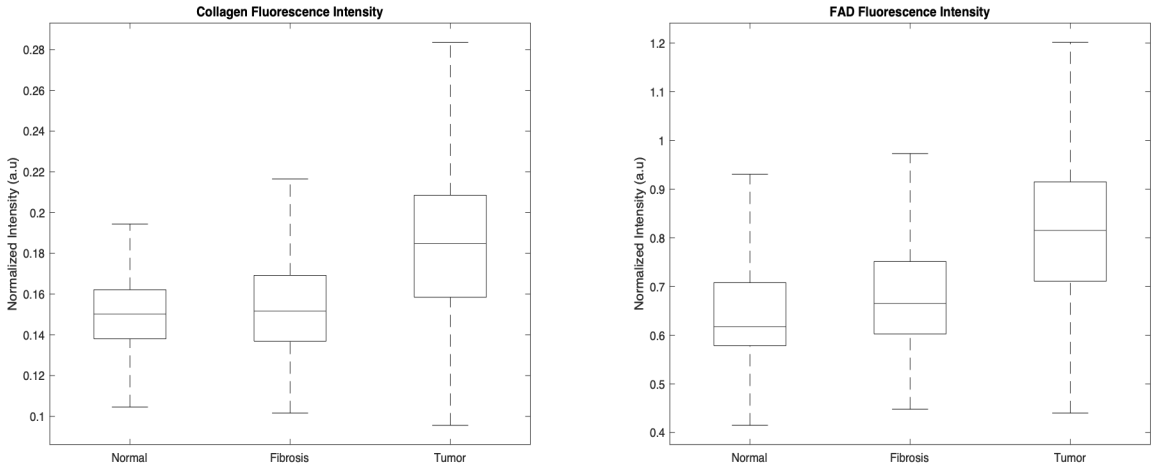

*Figure 4.2**: Box plots for normalized fluorescence intensity for collagen and FAD for each tissue type.***

Similar to the results for fluorescence lifetime there is a statistically significant difference between tumor and other tissue types in normalized fluorescence intensity for both fluorophores. Collagen intensity is higher in the tumor sample than the normal and fibrotic tissue which is expected based on how collagen is related to cancer [9]. One of the main characteristics of some cancers are increases in collagen in surrounding matrix. Collagen increases tissue stiffness, regulates immunity, and promotes metastasis for tumors [9]. This increase in collagen is demonstrated by the increase in normalized collagen intensity. Additionally, the normalized FAD intensity is also higher in the tumor compared to the normal and fibrotic tissue. The FAD intensity when normalized to NADH gives the redox ratio which is often used to describe metabolic changes in tissue. An increase in redox ratio, shown here in tumor tissue, shows a change in oxidative metabolism which is characteristic of cancer [10]. As mentioned previously the collagen make up within a tissue would increase with fibrosis progression and therefore the normalized collagen intensity would be greater in fibrotic compared to normal lung tissue. However, this may not be a statistically significant difference as this may be in early stages of fibrosis. Additionally, since there is a decrease in metabolism between fibrotic and normal tissue, a difference in redox ratio is present, a measure of metabolism within a tissue.

4.3 Diffuse Reflectance

Figure 4.3 shows the average diffuse reflectance extracted from the 0.64mm collection fibers with respect to wavelength for each tissue type. It can be seen from the graph that overall fibrotic and normal tissue have similar diffuse reflectance with normal being slightly larger than fibrotic.

Tumor tissue shows no overlap with both normal and fibrotic tissue. The region of interest is between 480 and 580nm as this is where hemoglobin absorption occurs. Within this region there is a large difference between tumor and other tissue types. This may be due to vasculature changes in tumor tissue compared to other tissue types.

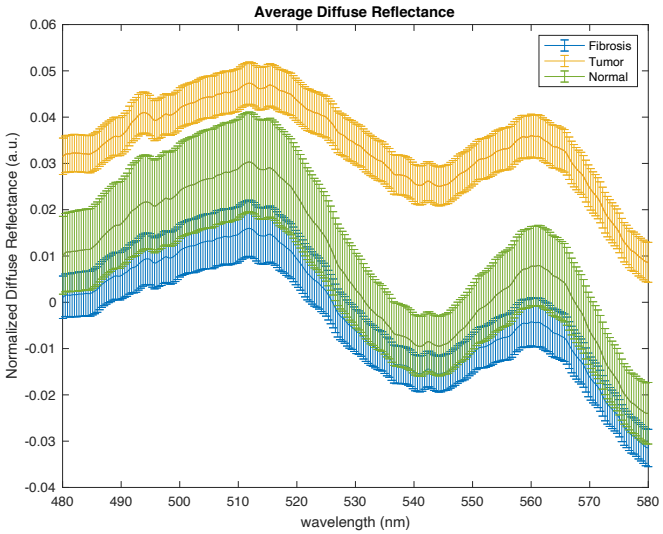

*Figure 4.3**: Average diffuse reflectance with respect to wavelength for each tissue type.***

4.4 Absorption and Reduced Scattering Coefficient

Figure 4.4 gives the average absorption coefficient with respect to wavelength for each tissue type. The average reduced scattering coefficient with respect to wavelength is displayed in figure 4.5. Absorption coefficients vary slightly between tissue types at the peaks which correspond to hemoglobin absorption. The reduced scattering coefficient varies significantly between tumor and the other tissue types. There are some differences particularly at larger wavelengths in reduced scattering coefficient between fibrotic and normal tissue.

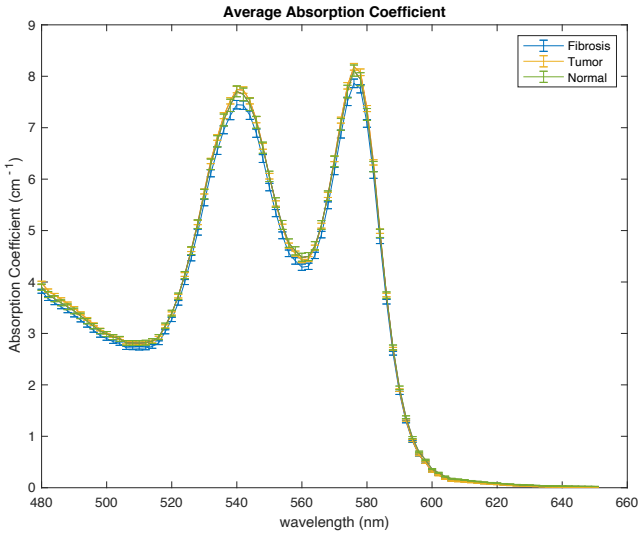

*Figure 4.4**: Average absorption coefficient with respect to wavelength for each tissue type.***

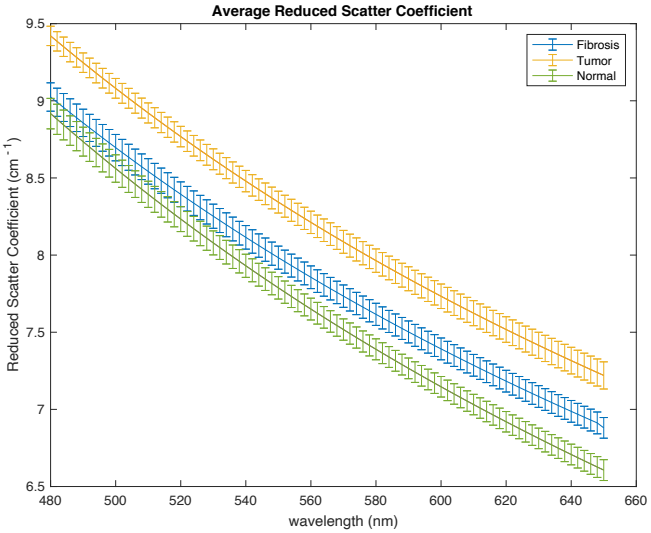

Figure 4.5**: Average reduced scatter coefficient with respect to wavelength for each tissue type.**

The reduced scattering and absorption coefficients at the wavelengths of interest, 540nm and 576nm for each tissue type are shown in Table 4.5. Table 4.6 gives the Wilcoxon ranked sum test results for these coefficients when comparing tissue types. Figures 4.6 and 4.7 show the histograms of the absorption and reduced scatter coefficient respectively for the wavelengths of interest for each tissue type.

Table 4.5: ***Reduced scattering and absorption coefficients (cm^{-1}) at 540nm and 576nm and standard deviation for each tissue type***

	Reduced Scattering Coefficient (cm^{-1})		Absorption Coefficient (cm^{-1})	
	540nm	576nm	540nm	576nm
Normal	7.95±0.6	7.45±0.6	7.72± 0.7	8.18± 0.6
Fibrotic	8.11±1.0	7.71±1.0	7.75±0.7	8.11±0.8
Tumor	8.48±1.2	8.01±1.3	7.85±0.7	8.27±0.6

Table 4.6: ***Wilcoxon ranked sum test results for reduced scattering and absorption coefficients (cm^{-1}) at 540nm and 576nm***

	Reduced Scattering Coefficient		Absorption Coefficient	
	540nm	576nm	540nm	576nm
Normal vs. Fibrotic	0.93	0.13	0.35	0.34
Fibrotic vs. Tumor	P < 0.01	P < 0.01	P < 0.01	P < 0.01
Normal vs. Tumor	P < 0.01	P < 0.01	0.1493	0.0306

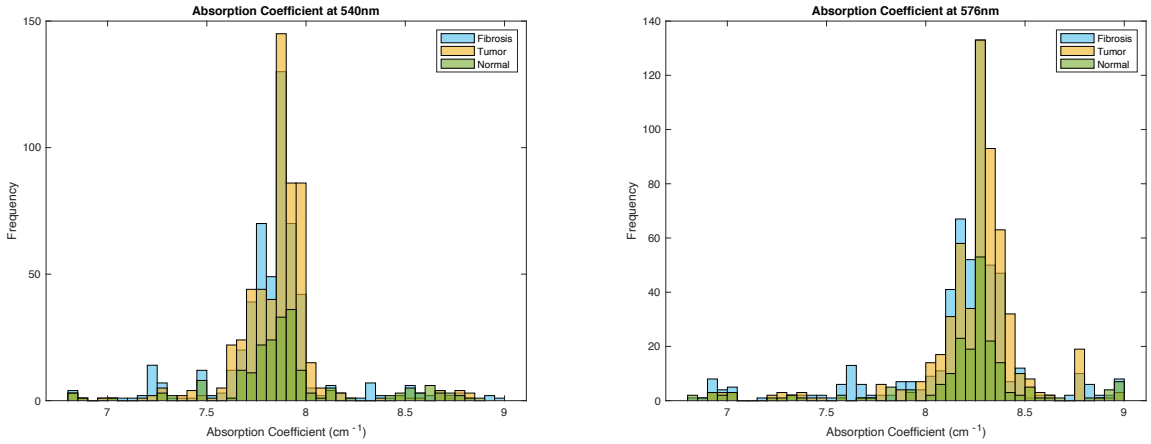

Figure 4.6: ***Histogram of absorption coefficient at 540nm and 576nm for each tissue type.***

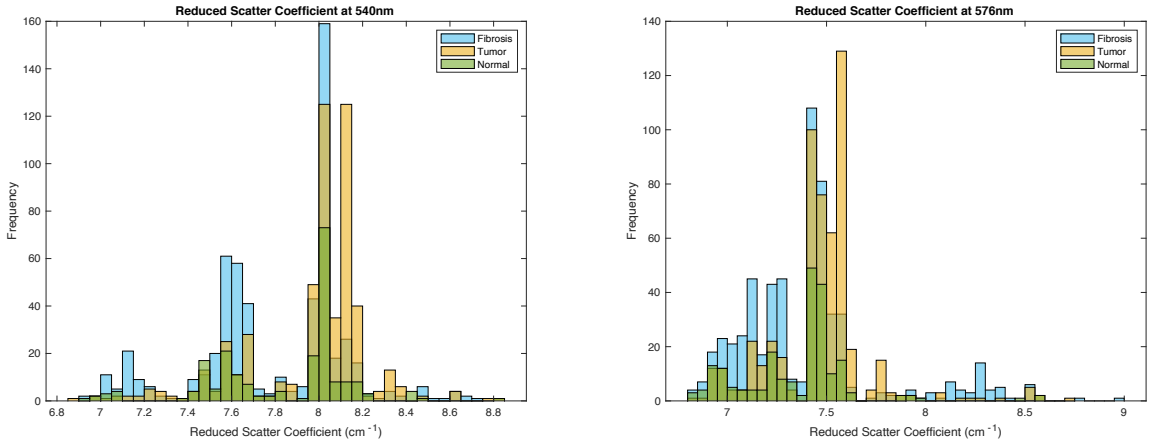

*Figure 4.7**: Histogram of reduced scatter coefficient at 540nm and 576nm for each tissue type.***

The absorption coefficients at both wavelengths, 540nm and 576nm, which corresponds to oxyhemoglobin absorption shows an increase for tumor compared to fibrotic and normal tissue. When considering that cancerous tissue creates more blood vessels to continue its growth compared to normal tissue [11] an increase in absorption coefficient is predicted. This increase in vasculature means more oxyhemoglobin is present which would be reflected as an increase in absorption coefficient at 540 and 576nm. The difference when comparing tumor to fibrotic tissue is statistically significant but is not when comparing to normal.

The reduced scattering coefficients at 540nm and 576nm are larger in tumor compared to fibrotic and normal tissue. A larger reduced scattering coefficient is correlated to more scattering occurring. An increase in scattering occurrence is linked to more cells and nuclei present in tumors compared to normal and fibrotic tissue. The results are statistically significant when comparing tumor to normal and tumor to fibrotic tissue.

For both the reduced scattering and absorption coefficients the normal and fibrotic tissue differences are not statistically significant. Given that scar tissue functions at a fraction of normal tissue this implies that some structures of the cells and matrix are similar between the two tissue types. If the structure of the tissue is still similar the absorption and reduced scattering coefficients may vary but not in a statistically significant manner. Based on the histograms the distribution for normal while having a smaller frequency than either of the other tissue types shows a pattern more similar to fibrotic than tumor.

References

[1] M. Wang, F. Tang, X. Pan, L. Yao, X. Wang, Y. Jing, J. Ma, G. Wang, L. Mi, "Rapid diagnosis and intraoperative margin assessment of human lung cancer with fluorescence lifetime imaging microscopy," BBA Clinical, Vol. 8, pp. 7-13. 2017.
[2] K. Awasthi, F. Chang, P. Hsieh, H. Hsu, and N. Ohta, "Characterization of endogenous fluorescence in nonsmall lung cancerous cells: A comparison with nonmalignant lung normal cells," Journal of Biophotonics, Vol. 13, pp. e201960210. 2020.
[3] M. Y. Berezin, and S. Achilefu. "Fluorescence lifetime measurements and biological imaging." Chemical Reviews, Vol. 110, pp. 2641-2684. 2010.
[4] D. Chorvat, and A. Chorvatova. "Multi-wavelength fluorescence lifetime spectroscopy: a new approach to the study of endogenous fluorescence in living cells and tissues." Laser Physics Letters, Vol. 6, pp. 175-193. 2009.
[5] T. M. Alfaro, and C. R. Cordeiro, "Comorbidity in idiopathic pulmonary fibrosis-what can biomarkers tell us?" Therapeutic Advances in Respiratory Disease, Vol. 14, pp. 1753466620910092. 2020.
[6] A. Atala, D. J. Irvine, M. Moses, and S. Shaunak, "Wound Healing Versus Regeneration: Role of the Tissue Environment in Regenerative Medicine," MRS Bull, Vol. 35, 2010.
[7] N. Shalaby, A. Al-Ebraheem, V. N. D. Le, S Cornacchi, Q Fang, T Farrell, P. Lovrics, G. Gohla, S. Reid, N. Hodgson, and M. Farquharson, "Time-resolved fluorescence (TRF) and diffuse reflectance spectroscopy (DRS) for margin analysis in breast cancer," Lasers in Surgery and Medicine, vol. 50, pp. 236-245. 2018.
[8] S. Ricard-Blum, G. Baffet, and N. Théret, "Molecular and tissue alterations of collagens in fibrosis," Matrix Biology, Vol. 68, pp. 122-149. 2018.
[9] S. Xu, H. Xu, W. Wang, S. Li, H. Li, T. Li, W. Zhang, X. Yu, and L. Liu, "The role of collagen in cancer: From bench to bedside," Journal of Translational Medicine, Vol. 17, 2019.
[10] M. Wang, F. Long, F. Tang, Y. Jing, X. Wang, L. Yao, J. Ma, Y. Fei, L. Chen, G. Wang, and L. Mi, "Autofluorescence Imaging and Spectroscopy of Human Lung Cancer'" Applied Sciences. Vol. 7, pp. 32. 2017.
[11] P. Vaupel, A. Mayer, and M. Höckel, "Impact of hemoglobin levels on tumor oxygenation: the higher, the better?" Strahlentherapie und Onkologie, Vol. 182, pp. 63-71. 2006.

Chapter 5: Conclusion

5.1 Major Findings

The BEAR system was used to measure optical properties from 20 patients diagnosed with squamous cell carcinoma and 9 normal lung tissue samples. Differences in optical parameters between tumor, fibrotic and normal lung tissue were investigated. All metabolic related parameters (FAD and NADH) showed differences across all three tissue types. Most optical parameters had a statistically significant difference between tumor and the other two tissue types. The exception was normal versus tumor for absorption coefficient which was not a statistically significant difference. Between the normal and fibrotic tissue there was no statistically

significant differences between the tissue types for the reduced scattering coefficient, absorption coefficient, normalized collagen intensity ratio, and collagen fluorescence lifetime. Theories for why this has occurred are found in the results section as other researchers have not separated these two tissue types when reviewing optical parameters for tumor margins.

5.2 Limitations and Future Work

This work used 100% tissue composition to analyze optical properties. During excision if there is any tumor left behind this means that there is a positive margin. Therefore, mixed tissue composition needs to be examined before using this system during surgery. In order to determine the composition, histology was taken of the sample and matched over a picture of the sample in the optical system. This matching may not have been perfect and histology processing may have slightly varied the tissue orientation which would lead to differences between histology and the optical system. Another limitation would be that this study uses single exponentials for TRF data fitting which is not what some researchers recommend. This means the calculated lifetimes and intensities may not be completely accurate. Given that the system is used for classification and results are compared to itself this is not an issue. If comparison of true values was required to compare to other works additional processing would be needed.

In future work this system could be moved to the surgical site to complete the same research in the same ambient lighting as the clinical application site and would also allow for fresh tissue to be used. If the results of this new study prove to be statistically significant the research can be taken a step further to *in vivo*. By completing *in vivo* research, the true value of the BEAR system would be determined in its clinical application setting. *In vivo* may result in differences in the optical properties and the thresholds for tumor would need to be adjusted accordingly. A study by Lukina et al. developed tissue preservation protocols to ensure that the fluorescence lifetime data of an ex vivo sample will show the same results as an *in vivo* sample [1]. Given the eventual implementation of this system during surgery Lukina et al. could be used as a guide for a new protocol. Lukina et al. was performed with two-photon excited fluorescence lifetime imaging (FLIM) microscopy and found that samples placed in 10% Bovine Serum Albumin (BSA) on ice immediately after excision showed the same fluorescence lifetimes and free versus bound protein ratios as those measured *in vivo*. This was only true up until 3 hours post excision. Averaging fluorescence lifetime across the cell may result in metabolic information loss [1] but may not be an issue in the case of this project. Additionally, this system has been used on breast

tissue and there may be further applications on other cancer types including brain and liver tissue.

5.3 Conclusion

In conclusion this work has shown that the BEAR system can be used to differentiate tumor from normal and fibrotic tissue. The optical properties have shown promise to assist surgeons during tumor excision to improve cancer margins.

References

[1] M.M. Lukina, L. E. Shimolina, N. M. Kiselev, V. E. Zagainov, D. V. Komarov, E. V. Zagaynova, and M. V. Shirmanova. "Interrogation of tumor metabolism in tissue samples ex vivo using fluorescence lifetime imaging of NAD (P) H," Methods and Applications in Fluorescence, vol. 8, pp. 014002. 2019.